ELSEVIER

Journal of Chromatography A, 807 (1998) 165–184

JOURNAL OF CHROMATOGRAPHY A

Characterization of large-pore polymeric supports for use in perfusion biochromatography

Duncan Whitney*, Mark McCoy, Neal Gordon, Noubar Afeyan

PerSeptive Biosystems, Inc., 500 Old Connecticut Path, Framingham, MA 01701, USA

Received 12 September 1997; received in revised form 19 January 1998; accepted 23 January 1998

Abstract

Perfusion chromatography is uniquely characterized by the flow of a portion of the column eluent directly through the resin in the packed bed. The benefits of this phenomenon and some of the properties of perfusive resins have been described before, and can be summarized as enhanced mass transport to interior binding sites. Here we extend the understanding of this phenomenon by comparing resins with different pore size distributions. Resins are chosen to give approximately the same specific pore volumes (as shown in the characterization section) but the varying contribution of large pores is used to control the amount of liquid flowing through the beads. POROS R1 has the largest contribution of throughpores, and therefore the greatest intraparticle flow. POROS R2 has a lower contribution of throughpores, and a higher surface area coming from a greater population of diffusive pores, but still shows significant mass transport enhancements relative to a purely diffusive control. Oligo R3 is dominated by a high population of diffusive pores, and is used comparatively as a non-perfusive resin. Although the pore size distribution can be engineered to control mass transport rates, the resulting surface area is not the only means by which binding capacity can be controlled. Surface coatings are employed to increase binding capacity without fundamentally altering the mass transport properties. Models are used to describe the amount of flow transecting the beads, and comparisons of coated resins to uncoated (polystyrene) resins leads to the conclusion that these coatings do not obstruct the throughpore structures. This is an important conclusion since the binding capacity of the coated product, in some cases, is shown to be over 10-fold higher than the precursor polystyrene scaffold (i.e., POROS R1 or POROS R2).

Keywords: Stationary phases, LC; Perfusion chromatography; Supports; Proteins

1. Introduction

Perfusion chromatography is characterized by both convective and diffusive solute transport within the internal pores of individual particles making up the chromatographic packed bed. At elevated flow-rates, since convective transport rates of larger biopolymers are several orders of magnitude greater than the diffusive rates, the interior binding sites within the pore network of perfusive supports are contacted more rapidly, than with packing materials relying solely on diffusive solute transport. It has been well documented that the rate of mass transport of biomolecules to interior binding sites is typically the dominant contribution to band broadening [1,2]. Accelerated mass transport resulting from intraparticle flow minimizes band broadening, which in turn is recognized as high column efficiency and high capture efficiency at elevated flow-rates. Perfusive supports [2,3] are characterized as having large,

*Corresponding author.

0021-9673/98/$19.00
PII: S0021-9673(98)00068-5

interconnected pores, with a complement of smaller pores, which contribute more heavily to high surface area. The relative contribution of these different populations of pores can be manipulated in order to optimize chromatographic behavior (e.g., band broadening and capacity).

Conventional biochromatography and high-performance liquid chromatography (HPLC) supports rely on high surface area, and hence high binding capacity, provided by an internal pore structure of pore sizes on the order of 10 to 100 nm [4–9]. These materials do not contain any intraparticle flow paths, such that mass transport to interior binding sites is limited by the rate of diffusion. The van Deemter equation clearly defines the loss of column efficiency as a function of flow-rate with these resins [1], such that high flow-rate operation is generally not feasible. Strategies that overcome slow diffusional transport by elimination of internal pores (e.g., membranes and non-porous particles) offer lower binding capacity and for this reason are not generally utilized for biomolecule purification. Perfusive supports combine the high binding capacity of conventional, high internal surface area particles, with the improved mass transport character of non-porous materials.

Modified forms of the van Deemter equation for perfusive supports have been developed [10,11] which define an operating regime where column efficiency becomes independent of flow-rate. The flow-rate at which this regime is achieved depends on the split ratio [12], defined as the ratio of flow which transects the particles to the flow through the packed bed. The split ratio, in turn, is related to the pore structure, which can be easily controlled during the synthesis process.

The properties of perfusive resins have been described before [2,3], and many applications where the benefits of fast chromatography are recognized have been reported. It has been shown [12] that only a small percentage of flow transecting the particles is required in order to recognize dramatic enhancements in mass transport rates. Here we will show the relationship of pore size distribution to particle permeability and binding capacity. Optimal pore size distributions have been identified based on these principles. This work focuses on the design, characterization and performance trade-offs of 20 μm diameter perfusive particles, although the same principles apply to other particle sizes.

The pore size distribution is critical to the unique intraparticle flow of perfusive resins. However, the binding capacity does not have to be controlled strictly by the ensuing effective surface area. The addition of surface coatings allows for fundamental change in the surface energetics when applied in a homogeneous manner and provides a means of controlling ligand density and binding capacity partially independent of the surface area. Once the optimal pore geometry for enhanced mass transfer is selected, surface chemistry optimization is able to deliver significantly higher binding capacity, than what would be predicted by the trade-offs of pore size and surface area inherent in macroporous polymer systems. However, to realize the full potential of this particle synthesis and coating approach, the coatings must be applied in a way that the intraparticle flow paths are not obstructed [13]. The basic notion is that the uncoated resin provides for the scaffolding for the surface derivatization chemistry.

2. Experimental

2.1. Materials

The chromatographic resins (POROS R1, POROS R2 and Oligo R3) were obtained in bulk quantity from PerSeptive Biosystems (Framingham, MA, USA). These were packed into columns as described below. POROS R and Oligo R3 represent underivatized poly(styrene–divinylbenzene) beads with varying pore size distributions, as described in the text below. POROS S, POROS SP, POROS HS (cation-exchange resins) and POROS HQ (anion exchanger) were obtained from PerSeptive Biosystems in bulk quantity and packed into columns as well. Comparisons of the ion-exchange resins with the POROS R materials reveals the contributions of the coating chemistries to the binding capacity and mass transport properties.

HEMA-IEC BIO 1000 SB was chosen as a purely diffusive control sample for comparison to POROS ion exchangers. This resin was purchased from Alltech Associates (Deerfield, IL, USA).

HPLC grade acetonitrile (ACN) part No. AX0145-1 and reagent grade tetrahydrofuran (THF) part No. TX0280-7 were purchased from E.M. Science (Gibbstown, NJ, USA). Reagent grade trifluoroacetic

acid (TFA) part No. T6220-0 and formic acid 96% A.C.S reagent part No. 25 136-4 were purchased from Aldrich (Milwaukee, WI, USA). Purified water was produced in-laboratory.

Lysozyme, part No. L-6876; bovine serum albumin (BSA), part No. A-7906; and human γ-globulin (hIgG), part No. G-4386 were purchased from Sigma (St. Louis, MO, USA). The molecular mass and free molecular diffusivities of these proteins are given in Table 1.

Polystyrene (PS) standards were obtained from Supelco (Bellefonte, PA, USA) and Polysciences (Warrington, PA, USA). These standards ranged in molecular mass from 250 to 30 000 000.

2.2. Instrumentation

The frontal and zonal chromatography experiments were performed using a BioCAD™ Perfusion Chromatography Workstation (PerSeptive Biosystems). The instrument includes an integrated UV–Vis detector equipped with a 9-μl flow cell having a path length of 6 mm. Actual flow-rates were measured for each experimental flow-rate.

The mercury porosimetry measurements were carried out on a Micromeritics PoreSizer 9320 version 2.01 (Micromeritics, Norcross, GA, USA).

Inverse size-exclusion measurements were conducted on an Hewlett-Packard Model 1090L HPLC system (HP-1090L) (Hewlett-Packard, Palo Alto, CA, USA), and controlled by personnel computer using HP-Chemstation software. The HP-1090L is capable of delivering precise, accurate flow-rates up to 5.0 ml/min.

The scanning electron micrographs were taken with the Topcon Model 510 scanning electron microscope (Topcon, Tokyo, Japan).

Columns were packed using a Shandon column packer (Shandon Southern Products, Astmoor, Runcorn, UK).

Table 1
Molecular mass (M_r) and free molecular diffusivity (in water at 20°C) of the protein samples [41]

Protein	M_r (Da)	$D \cdot 10^{11}$ (m^2/s)
Lysozyme	13 930	11.2
BSA	67 000	5.9
hIgG	153 100	4.0

2.3. Procedures

2.3.1. Column packing

All columns were packed at a constant pressure of 180 bar on a Shandon column packer using a ACN–water (20:80) push solvent. The frontal experiments were conducted using 100×3.2 mm stainless steel columns sealed with 0.5-μm polyether ether ketone (PEEK) frits. The van Deemter measurements were conducted using 100×4.6 mm PEEK columns sealed with 2.0-μm PEEK frits. Only those columns passing the requisite efficiency and asymmetry specifications were used in latter experiments. The inverse size-exclusion (i-SEC) experiments were conducted using 250×4.6 mm stainless steel columns sealed with 2-μm stainless steel frits.

2.3.2. Frontal analysis

Frontal breakthrough curves were measured for feeds consisting of 1.0 mg/ml of lysozyme, BSA or hIgG in water+0.1% TFA; on columns packed with POROS R1, POROS R2 or Oligo R3; at flow-rates of 0.25, 0.5, 1.0, 3.0 and 5.0 ml/min; and at ambient temperature (20±2°C). The adsorbate was detected using the integrated UV–Vis detector set at 250 nm for hIgG and lysozyme, and 280 nm for BSA. the experiments were conducted on a BioCAD Perfusion Chromatography Workstation.

The method consisted of equilibrating the column with 10 column volumes (CVs) of buffer (water+0.1% TFA). After taking the column off-line the system was purged with 10 ml of feed (1.0 mg/ml adsorbate in water+0.1% TFA). The column was then brought on-line and loaded with feed until at least 95% breakthrough was achieved. Excess feed was washed out of the column with 5 CVs of buffer. The adsorbate was eluted using 30 CVs of eluent [ACN–water (95:5)+0.1% TFA] in combination with a 1.5-ml injection of formic acid after 5 CVs of elution. After re-equilibrating the column with 30 CVs of buffer, the column was ready for the next run.

The feed solutions were filtered using a 0.45-μm cellulose acetate filter (VWR Scientific, Boston, MA, USA). The feed, buffer and eluent were degassed by sonicating the solution while applying vacuum.

From the breakthrough curves, dynamic capacities were calculated in accordance with,

$$C_{5\%} = \frac{(t_{5\%} - t_0)}{V_c} F C_{d,in} \quad \text{and}$$

$$C_{50\%} = \frac{(t_{50\%} - t_0)}{V_c} F C_{d,in} \tag{1}$$

where $C_{5\%}$ is the dynamic capacity at 5% of breakthrough, $C_{50\%}$ is the dynamic capacity at 50% of breakthrough, $t_{5\%}$ is the time of 5% breakthrough, $t_{50\%}$ is the time of 50% breakthrough, F is the volumetric flow-rate, $C_{d,in}$ is the adsorbate concentration in the feed, V_c is the volume of the column (0.804 ml), and t_0 is the retention time of a non-retained tracer. The equilibrium uptake, $C_{s,eq}$, was estimated as $C_{50\%}$ at $F = 0.25$ ml/min.

2.3.3. Zonal analysis

Experimental van Deemter curves were measured for a sample consisting of 1.0 mg/ml of lysozyme in ACN–water (50:50)+0.1% TFA; on columns packed with POROS 20 R1, POROS 20 R2 or Oligo R3; at flow-rates of 0.5 to 13.0 ml/min. Temperature was controlled at 30°C by placing the column in a column oven and by placing the eluent reservoirs in a circulating water bath. The adsorbate was detected using the integrated UV–Vis detector set at 215 nm.

The experiments were conducted on a BioCAD Perfusion Chromatography Workstation plumbed with minimal lengths of 0.005 in. diameter PEEK tubing, which minimizes extra-column dispersion (1 in. = 2.54 cm). The eluent, ACN–water (50:50)+ 0.1% TFA, was chosen to ensure that the lysozyme sample is not retained on the media. The column was equilibrated with 2 CVs of eluent. Upon equilibration a 5-μl lysozyme sample was injected via a 10-μl injection loop. The sample was eluted from the column with 2 CVs of eluent.

The experimental values of the height equivalent to a theoretical plate (H) were calculated in the BioCAD software according to the following formulas,

$$N = 2\pi\left(\frac{h' t_r}{A}\right)^2 \quad \text{and} \quad H = \frac{L_0}{N} \tag{2}$$

where N is the number of theoretical plates, t_r is the retention time, h' is the peak height, A is the peak area and L_0 is the length of the column. The delay volume was measured by injecting 1 μl of acetone–eluent (50:50) solution via the injection loop; while a zero dead volume union was substituted for the column. The retention time was corrected for the measured delay volume.

Values of the split-ratio (α) and tortuosity factor (τ) were estimated by using non-linear regression to fit a theoretical expression for the van Deemter curve to the experimental van Deemter curve. A detailed description of this method as applied to perfusive or potentially perfusive media is presented in Ref. [12]. The split ratio is the volumetric fraction of mobile phase flowing through the particle relative to the volumetric flow-rate through the column. It is given by,

$$\alpha = \frac{F_p}{F} \tag{3}$$

where α is the split ratio, F is the volumetric flow-rate of the mobile phase flowing through the column, and F_p is the volumetric flow-rate of the mobile phase passing through the media. The tortuosity factor, τ, is defined by,

$$D_p = \frac{D}{\tau} \tag{4}$$

where D_p is the effective pore diffusivity and D is the free molecular diffusivity (see Table 1).

2.3.4. Size-exclusion

i-SEC experiments were conducted using an HP-1090L HPLC system; on columns packed with POROS 20 R1, POROS 20 R2 or Oligo R3. Distribution coefficients (K_d) were determined for polystyrene standards. The standards ranged in molecular mass from 250 to 30 000 000. The mobile phase was THF, and the temperature set at 35°C. The flow-rate was set to 0.2 ml/min to prevent shear force degradation of the larger PS standards. After equilibrating the column with 2 CVs of THF, a 25-μl sample of PS standard was injected. The sample was eluted with 2 CVs of THF and detected at 240 nm on the HP-1090L diode array detector.

The distribution coefficients were calculated according to the following expression,

$$K_d = \frac{t - t_0}{t_p} \tag{5}$$

where t is the retention time for the PS standard being tested, t_0 is the retention time at the exclusion limit, and $t_p + t_0$ is the retention time for the smallest molecule that can penetrate all the pores with the probability equal to one.

2.3.5. Hg porosimetry

Mercury porosimetry measurements were conducted on POROS 20 R1, POROS 20 R2 and Oligo R3 using a Micromeritics PoreSizer 9320. Experiments were conducted in accordance with the protocol given in the PoreSizer 9320 operator's manual [14], using a maximum pressure of 30 000 p.s.i. (1 p.s.i. = 6894.76 Pa). The pore size calculation is according to the following equation,

$$D = \frac{-4\gamma\cos\theta}{P} \quad (6)$$

where, θ, is the contact angle of mercury, γ, is the surface energy of mercury, and, P is the pressure required to force the mercury into a pore of diameter, D.

3. Results and discussion

3.1. Description of perfusive resins

The control of pore size distribution of conventional chromatographic supports is important due to the relationship of pore size and surface area to binding capacity. In the case of flow-permeable supports, for perfusion chromatography, the control of pore size becomes more important due to the unique and added role of the population of large diameter, interconnected throughpores. Models describing the permeability of individual perfusive particles [11,15] and examination of the Carmen–Kozeny equation (Eq. (11)), lead to the prediction that small changes in pore size and pore volume can lead to substantial changes in the intraparticle permeability. Since perfusion can be defined by the ratio of particle permeability to packed-bed permeability, or split ratio, this predictability underscores the importance of pore size control with these supports. The discussion below, involving comparisons of supports of varying pore size, demonstrate the relationships of pore size distribution to split ratio and convectively enhanced mass transport such that one can ultimately relate chromatographic performance to the morphology of the resins.

POROS R1, POROS R2 and Oligo R3 are made by a styrene–divinylbenzene suspension co-polymerization process, with an aqueous-based continuous-phase (the particles described here are all 20 μm in diameter, unless otherwise noted). Control of the pore size distribution in POROS resins is similar to systems that have been described before [16–22]. Reviews of the proposed mechanisms [19,22,23] are useful for description of the variables affecting pore morphologies. Perfusive resins are engineered to have a very broad pore size distribution allowing for a mix of large interconnecting pores (i.e., 10 000–5000 Å), that serve as the intraparticle flow channels, and a population of smaller diffusive pores (i.e., 500 Å) that contribute more significantly to the specific surface area. Individual particles are composed of agglomerated microspheres (as described by others [18–20,22]). Void spaces between the microspheres and agglomerates define the pore size distribution of individual particles. In the case of POROS resin channels as large as 1 μm (as seen in Figs. 1 and 2) separate the agglomerates. Although the precise method by which the POROS resins are made is not included, the pore morphology of these resins is enumerated below allowing a correlation of structure to some of the unique chromatographic mass transport properties.

3.2. Particle physical property and mass transport relationships

The nature and benefits of perfusion chromatography, based on the resins described below in detail, have been extensively examined in both theoretical [2,11,24–28] and application specific [29–32] references (some of which are listed here). The theoretical work describes how the column efficiency becomes independent of flow-rate in the perfusive regime, in contrast to conventional resins where efficiency is continually compromised as flow-rate is increased. The onset of the perfusion regime, however, can be variable, depending on the split ratio, as defined above. In frontal mode the perfusive regime is characterized as a preservation of binding capacity with increasing flow-rate. In zonal mode column

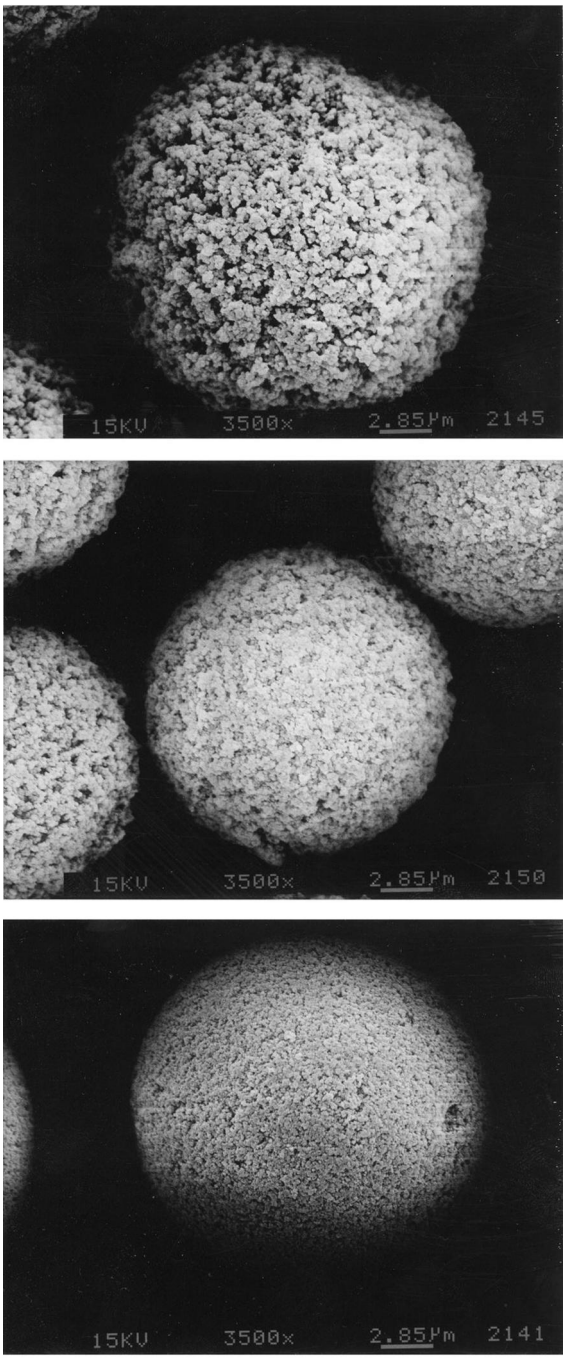

Fig. 1. SEM of POROS R1, POROS R2 and Oligo R3. Low magnification (3500×) scanning electron microscopy reveals gross differences in the pore morphologies of POROS R1 (top), POROS R2 (middle) and Oligo R3 (bottom). The scale-bar represents 2.85 μm.

efficiency is maintained with increasing flow-rate for separation of mixtures. However, in both cases, the degree of convective enhancement of the mass transfer will depend on the degree of intraparticle flow and therefore the particle design.

The rigid structure of POROS resins readily lend themselves to direct pore size distribution measurements. Included below is data from a variety of measurement techniques, comparing POROS R1, POROS R2 and Oligo R3, showing the effects of pore size distribution on mass transport behavior. It is also possible to efficiently coat the available surfaces of POROS resins, as described in detail by Varady et al. [13] which can dramatically impact both the selectivity and the binding capacity of the resulting resins. The addition of coatings gives us added degrees of freedom to be able to gain high biomolecule binding capacity even for very large pore-size, relatively low surface area, perfusive supports.

Characterization of pore morphology using mercury porosimetry yields values of specific pore volume, V_{sp} (ml/g), nominal pore size [D_{pore} (Å)], and specific surface area, A_{sp} (m^2/g). Porosimetry results for multiple lots of POROS R1, POROS R2 and Oligo R3 are summarized in Table 2. The total pore volume is measured from the cumulative intrusion volume curve, and the nominal pore size is taken as the peak in the differential intrusion curve. The specific surface area value is calculated from the cumulative intrusion curve, assuming a cylindrical pore model. Significantly higher surface area values by gas-adsorption (BET) measurements have been observed [e.g., 124 m^2/g for a selected POROS R2 lot (data not shown), as opposed to 72.5 m^2/g by porosimetry]. There is a fundamental difference in the way surface area values are derived by the two techniques, nitrogen can be adsorbed into smaller pores than the non-wetting mercury can access, even at very high pressures. However, porosimetry derived surface area values are more useful for correlating pore morphology to biomolecule adsorption and capacity measurements. The surface area that is available to adsorption of proteins, for instance, is relative to the size of the pores, and the presence of microporosity that can be measured by nitrogen adsorption tests, is not a good indicator of the protein binding capacity.

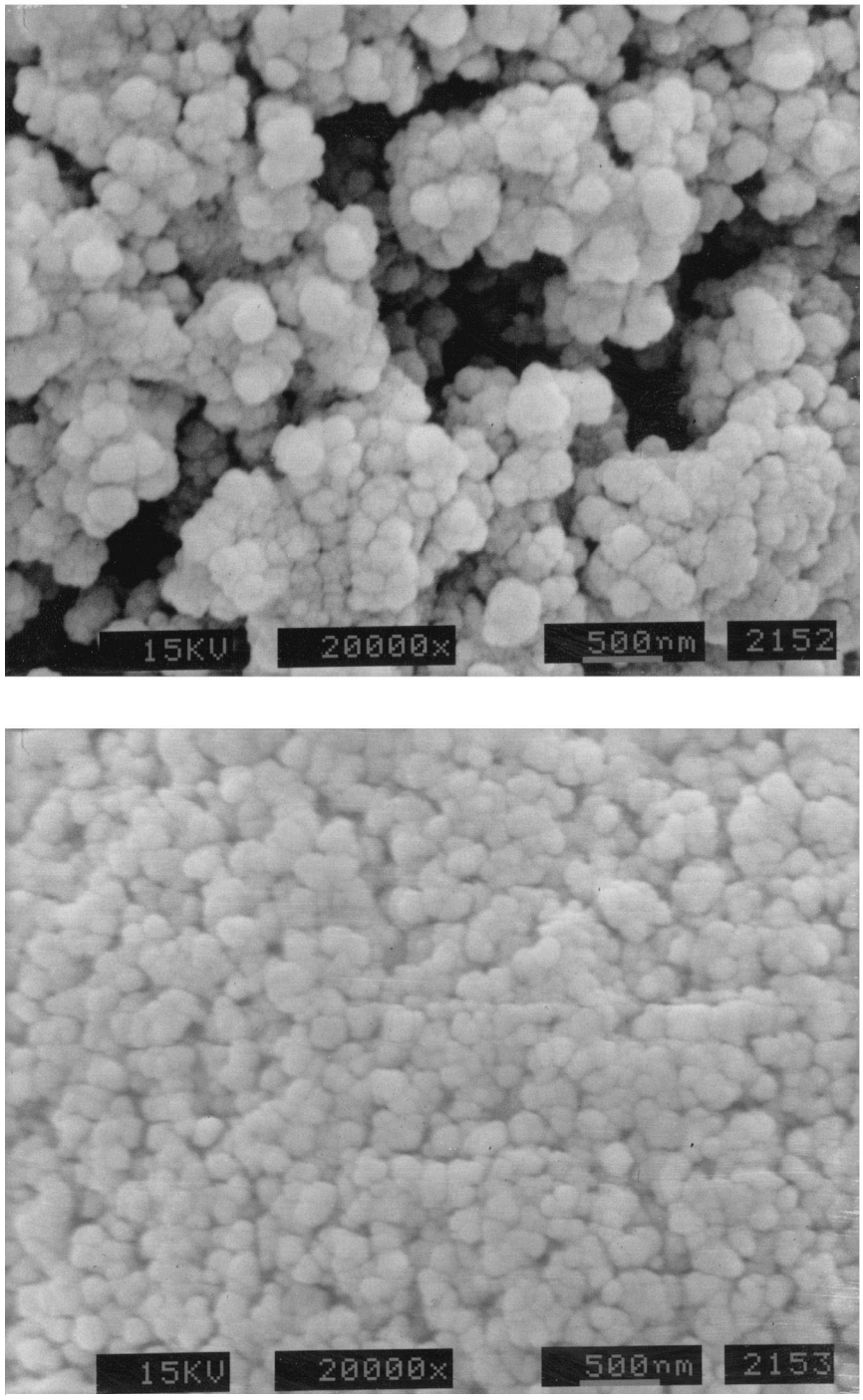

Fig. 2. SEM of POROS R1 and Oligo R3. High magnification (20 000×) SEM of POROS R1 (top) and Oligo R3 (bottom), shows the dramatic differences in the population of large pores of a perfusive and non-perfusive resin, respectively. The scale-bar represents 0.5 μm (5000 Å). The POROS R1 has a lower pore volume than the Oligo R3, such that the difference in pore size arises from the difference in the homogeneity of microsphere agglomeration.

Table 2
Porosimetry results of POROS R1, POROS R2 and Oligo R3, as described in Section 3.2

Batch	V_{sp} (ml/g)	D_{pore} (Å)	A_{sp} (m^2/g)	N (batches tested)
POROS R1	1.50±0.01	2945±175	44.6±5.0	5
POROS R2	1.80±0.07	1540±172	72.5±5.0	11
Oligo R3	1.72±0.03	210±0.0	171±1.0	3

The resins are characterized by specific pore volume (V_{sp}), average pore diameter (D_{pore}) and specific surface area (A_{sp}), using the software supplied with the instrument. The number (N) of lots of resin tested is also specified.

The nominal pore size of the Oligo R3 is 210 Å as measured consistently on three lots. This is consistent with other commercially available polymeric and silica-based supports for use in biomolecule chromatography. The POROS R2 has a nominal pore size of almost an order of magnitude greater than the Oligo R3, the non-permeable control. The POROS R1, has a nominal pore size that is about twice as large the POROS R2.

The porosity (ε_{pore}) of the resins can be calculated from the cumulative specific pore volume according to the following equation,

$$\varepsilon_{pore} = \frac{V_{pore}}{V_{pore} + V_{polymer}} = \frac{V_{sp}}{V_{sp} + (\rho_{polymer})^{-1}} \quad (7)$$

The density of the polymer, $\rho_{polymer}$, is 1.05 g/ml. The porosity, calculated from the average V_{sp}, for 11 lots of POROS R2 (Table 2), is 0.654. The porosity values for POROS R1 and Oligo R3 are, 0.61 and 0.64, respectively. The porosity values for all three resins are similar. But it is noteworthy that the POROS R1, which has been shown to have the highest split ratio [12], has the smallest porosity, suggesting that the population of large throughpores is responsible for the high intraparticle permeability.

Scanning electron microscopy (SEM) confirms the variation in pore sizes of the POROS R1, POROS R2 and Oligo R3, as shown in Figs. 1 and 2. It is also apparent from the high magnification (20 000×) micrographs that perfusive resins, with POROS R1 as an example, have broad pore size distributions, with pores ranging from several thousand angstroms (separating microsphere agglomerates) to a few hundred angstroms (spaces between the microspheres themselves). The high magnification of Oligo R3 does not reveal the same population of large pores. Examination of fractured particles, and independent transmission electron microscopy (TEM) analysis [33], with each of these samples, confirms that the morphology is consistent from the surface to the interior. However, POROS R1, POROS R2 and Oligo R3 have similar pore volumes (as shown by the porosimetry results). Therefore, the differences in pore size and resulting mass-transfer characteristics are due to differences in microsphere agglomeration density, as seen in Fig. 2. The more tightly the microspheres are agglomerated, the more space is left between microsphere agglomerates (as with POROS R1). On the other hand if the microspheres are more loosely agglomerated, more of the surface of the individual microspheres is available for contributing to the total specific surface area, but less space is available for large pores and fast accessibility to those surfaces (as with Oligo R3). The size of the actual microspheres, comparing POROS R1 and Oligo R3 (Fig. 2), are about the same (100–200 nm).

Porosimetry is readily adapted to the accurate measure of pore volumes, but requires high pressures, and may not give the most accurate representation of the surface area, as mentioned above. Gas-adsorption techniques, on the other hand, are generally accepted means of accurately assessing surface area, but are not reliable for measuring porosity of large pore materials (e.g., >500 Å, nominal pore size). Inverse size-exclusion [34–37], however, is an alternative means of characterizing large pore materials and was applied here to confirm the pore size differences of the porosimetry analysis, above. The POROS R1, POROS R2 and Oligo R3 were packed into columns for size-exclusion characterization using monodisperse polystyrene standards, and low flow-rates. Using a broad range of molecular mass standards it is possible to compare the entire pore size distribution of each of the samples (Fig. 3). For instance, with the M_r 900 000 marker, there is

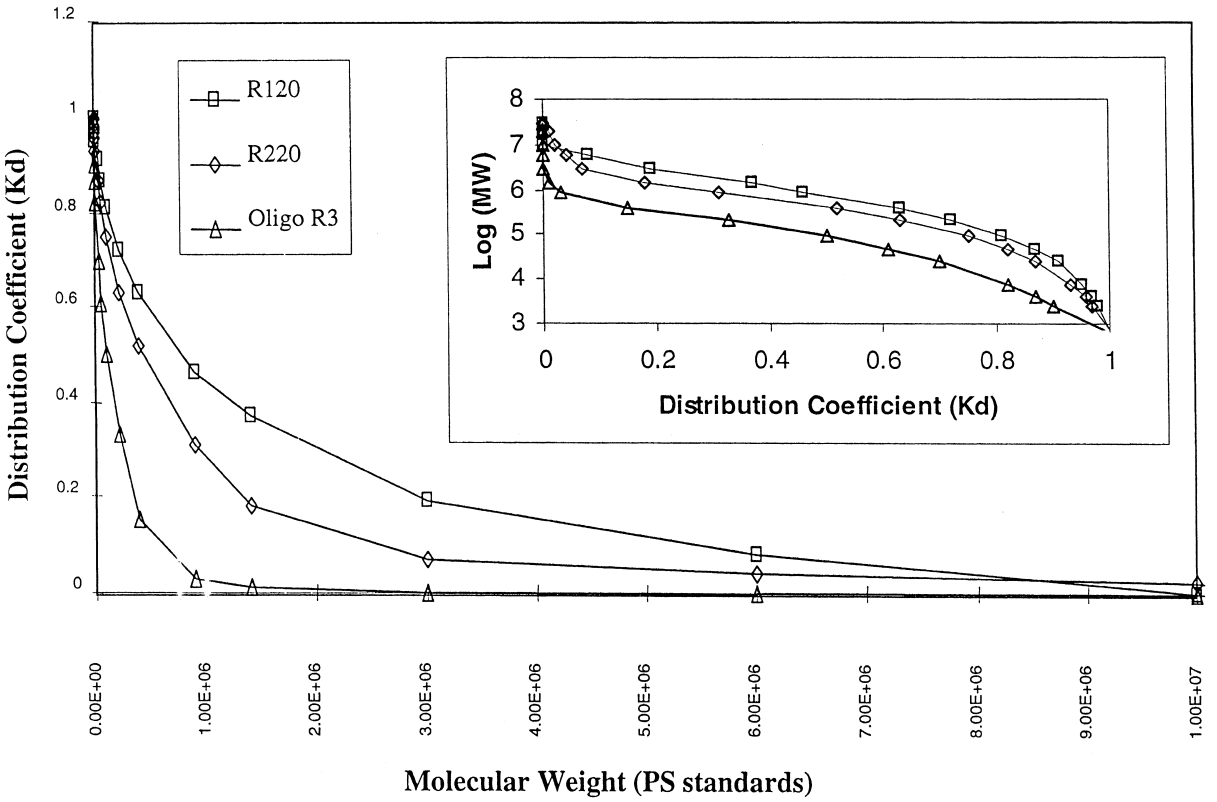

Fig. 3. Inverse size-exclusion analysis of resin pore size distribution. The plot of the molecular mass of the PS standards versus the distribution coefficient (K_d), as defined in Section 2.3.4, shows the differences in the accessibility of different sized probes, under chromatographic conditions, of the POROS R1, POROS R2 and Oligo R3. A plot of log (M_r) versus K_d (inset), is also a common means of relating pore size distributions.

only a very small percentage of pores (<5%) of sufficient size that are available in the Oligo R3 sample. By comparison, 30% of the pores are available in the POROS R2, and almost 50% with the POROS R1. Whereas, the exclusion limit for Oligo R3 is around 10^6, which is not unusual for conventional wide-pore supports, the exclusion limit is between 10^6 and 10^7 for POROS R2, and about 10^7 for POROS R1, although in the latter case the exclusion limit is not as well-defined. It is also possible to confirm the porosity data derived from the porosimetry experiments as follows. Assuming that the smallest probe (M_r 250) can access all of the pore space ($K_D = 1$), and that the largest (M_r 30 000 000) can access only the interstitial spaces ($K_D = 0$), then the total pore volume (V_p) can be described as the difference in the retention volumes of the two probes,

$$V_{pore} = (V_{PS250} - V_{PS30M}) = V_T - V_0 \quad (8)$$

The total volume of the particles ($V_{particle}$) is equivalent to the difference of the column volume (V_{column}) and the interstitial volume (V_0), and the porosity (ε_{pore}) is defined as the ratio of pore volume to particle volume,

$$V_{particle} = (V_{column} - V_0) \quad (9)$$

$$\varepsilon_{pore} = (V_{pore}/V_{particle}) \quad (10)$$

For example, with POROS R2, using values of

1.56, 1.72 and 4.15 for V_p, V_0 and V_{column}, respectively, a porosity of 0.64 is calculated, which compares favorably with the value derived by porosimetry.

In some early descriptions of perfusive resins [2] the permeability of individual particles was calculated based on some conservative estimates of porosity and microsphere size, treating the particle as a loosely packed agglomerate of smaller microspheres. More recently, refined models [38] have been applied toward the calculation of POROS permeability [POROS Q/M, (an anion-exchange functionalized resin in this case)]. A permeability value of $1.63 \cdot 10^{-15}$ m^2 was calculated from frontal analysis data using a Langmuir isotherm model, and a similar value was calculated from unretained protein data in conjunction with a van Deemter model [38]. Direct measures of intraparticle flow in POROS has been reported by Pfieffer et al. [15] using a specially developed apparatus for examining individual particles. Permeability values were then calculated from the flow data [15]. The confirmation of intraparticle flow in the typical back-pressure regime of HPLC systems is confirmation of the nature of the pore morphologies that have been previously described by models alone [2]. It is also a good verification of the accuracy of the perfusion models that were first proposed [2]. This latter point is made more clear, below, by refining some of the calculations made in Pfieffer et al.'s work with experimentally measured properties of the POROS particles in place of the approximate measures for microsphere size (d_m), and particle porosity (ε_p).

The direct measurements of intraparticle flow are reported to yield similar particle permeability values using air and water as permeate, after accounting for the differences in viscosity [15]. This is based on the following (Carmen–Kozeny) expression,

$$K = \frac{\varepsilon^3 d_m^2}{150(1-\varepsilon)^2} \tag{11}$$

The authors' conclusion is that the microspheres, defining the particle composition, must not be randomly arranged since the measured permeability ($K = 7.89 \cdot 10^{-15}$ m^2) is roughly an order of magnitude greater than the calculated value ($K = 0.46 \cdot 10^{-15}$ m^2) based on some approximations of microsphere size and porosity (i.e., $d_m = 0.37$ μm and $\varepsilon_p = 0.5$). However, the expression for the microsphere size may have been underestimated in the case of their theoretical model. In that discussion [15] the microsphere size is estimated from a specific surface area measurement (nitrogen adsorption and BET analysis), assuming a random arrangement of microspheres. In the descriptions of the particle morphology, above, it is actually the microspheres agglomerates that define the throughpore size (not the microspheres themselves). As a result, a relationship between specific surface area and pore size is not expected. Alternatively, a value of $\varepsilon_p = 0.61$ for POROS R1, calculated from porosimetry data in Table 2, and $d_m = 0.75$ μm (from SEM and TEM [33] analysis), where d_m is taken as the size of the microsphere agglomerate, in this context, an intraparticle permeability of $5.6 \cdot 10^{-15}$ m^2 is calculated, which is close to the experimentally derived value. Previous descriptions [2] of d_m assume that it is directly related to the resin pore size as follows:

$$d_m = 2d_{pore} \tag{12}$$

Based on pore size data in Table 2 (for POROS R1) values of $d_m = 0.60$ μm and $K_p = 3.6 \cdot 10^{-15}$ m^2 are calculated. This is still about almost an order of magnitude greater than the value based on assumed porosity and microsphere size [15], and is close to the directly measured value. In general, it is concluded that the description of intraparticle flow by a Carmen–Kozeny model is accurate, taking the size of the agglomerates of the microspheres as the parameter defining the intraparticle flow channels.

3.3. Dynamic binding capacity measurements

Frontal analysis data, with proteins, indicates the dynamically available binding sites. POROS R1 is expected to have a lower binding capacity based on the data summarized in Table 2, but the POROS R1 and coated supports prepared from it are expected to retain breakthrough capacity at elevated flow-rates due to the large population of throughpores. The Oligo R3 is used as a non-perfusive control in these comparisons. Frontal analysis is also a convenient means of demonstrating the increase in capacity upon introducing surface coatings. Coated resins have higher binding capacity than the underlying

polystyrene support (as described below), despite a lower measured surface area.

Breakthrough capacities are calculated from the point at which dynamically accessible binding sites are saturated, and the protein solution front begins to emerge from the column. The dynamic capacity is expected to be a function of the equilibrium capacity, the speed at which the solution moves through the packed bed, and internal and external mass transport resistance within the bed. With conventional resins where proteins must diffuse to internal binding sites, the entire binding capacity, as determined at the point of column breakthrough, is only recognized at very low flow-rates. As the flow is increased the rate of diffusion limits saturation of binding sites. As a result the dynamic capacity is compromised at elevated flow-rates [39]. In the case of perfusive supports, the effective diffusivity [2] is augmented by the intraparticle flow, with the amount of intraparticle flow dictated by the pore structure of the bead. The same concept of enhanced diffusivity has been previously demonstrated by Rodrigues et al. [40] for catalyst supports. In perfusion mode the breakthrough capacity does not deteriorate as quickly with flow-rate, and actually stabilizes at high flow-rates, whereby the dynamic capacity appears to become independent of flow-rate. Furthermore, the models [12] predict that perfusive supports with higher split ratios reach this stabilization point at lower flow-rates. In addition, the effect of convective enhancement (relative to purely diffusive mass transport rates) is expected to be greatest for larger biomolecules with the smallest diffusion coefficients (see Table 1).

A comparison of the breakthrough capacities as a function of flow-rate for POROS R1, POROS R2 and Oligo R3 are shown in Figs. 4–6 using the proteins lysozyme, BSA and hIgG, respectively. Fig. 4 demonstrates that the non-permeable Oligo R3, with the highest surface area of the three particles,

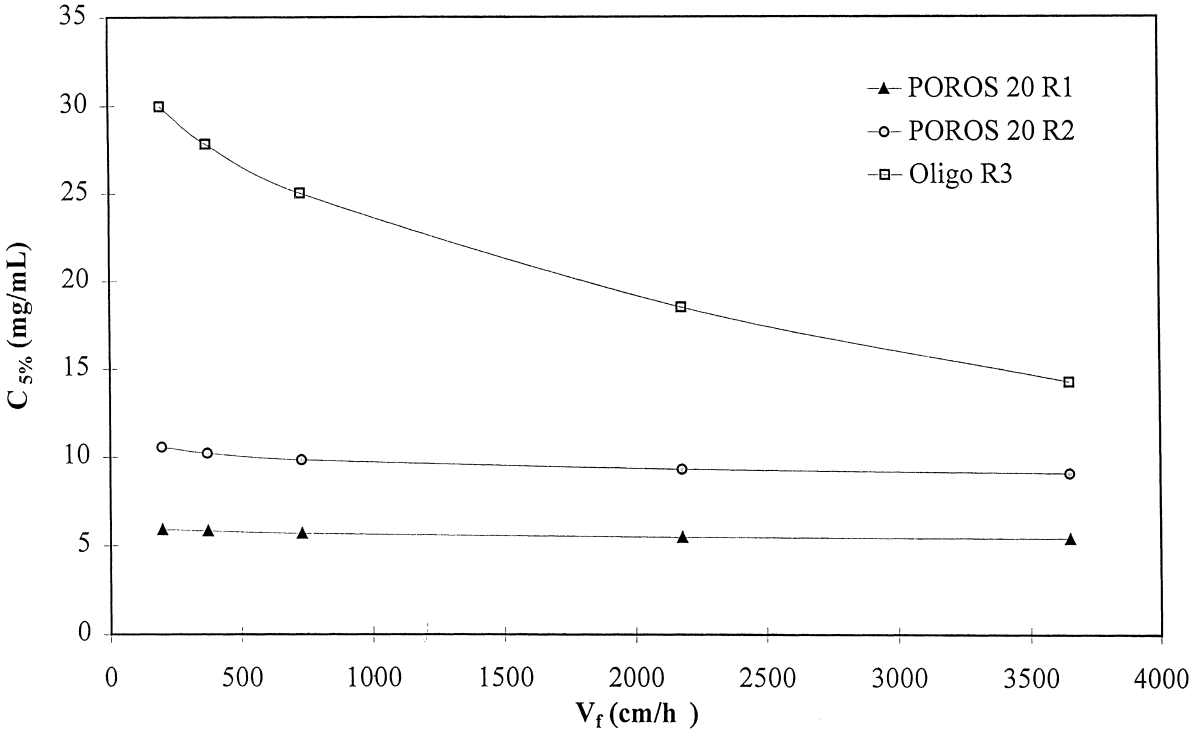

Fig. 4. Dynamic capacity comparisons using lysozyme. Dynamic capacity is expressed as the breakthrough capacity (at the 5% saturation point of the frontal curve). The dynamic capacity of POROS R1 and POROS R2 is virtually constant as a function of flow-rate. The dynamic capacity of Oligo R3 decreases as the flow-rate is increased.

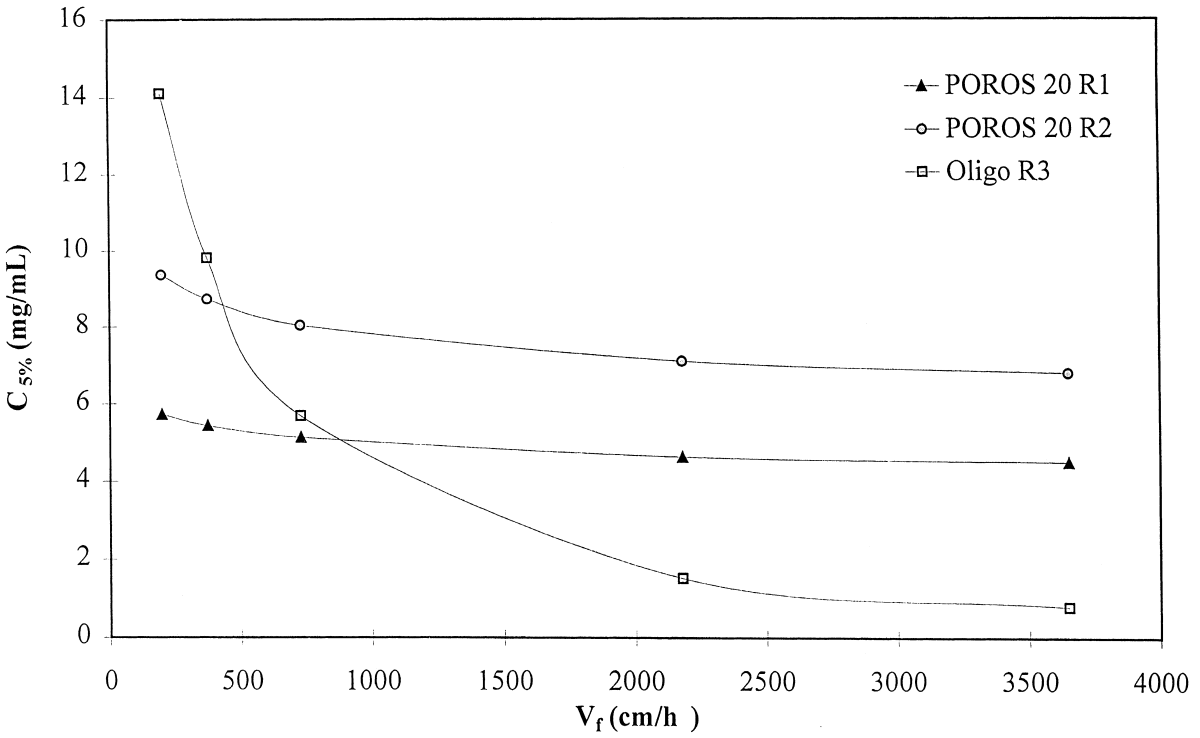

Fig. 5. Dynamic capacity comparisons using BSA. The dynamic capacity of POROS R1 and POROS R2 and Oligo R3 is shown as a function of flow-rate. The BSA has roughly 5× higher molecular mass than lysozyme and about 50% the free molecular diffusivity. These differences in the protein size and mobility affect the dynamic capacity characteristics of the non-perfusive Oligo R3 more dramatically than with either of the perfusive resins.

has superior binding capacity for lysozyme. As the superficial velocity is increased up to 3500 cm/h, the breakthrough capacity is compromised by 50%. The perfusive particles, POROS R1 and POROS R2, demonstrate very different dynamic capacity behavior. In the reversed-phase chromatography mode, due to the lower surface area, the capacity is lower than that of Oligo R3. However, due to convectively enhanced mass transfer, the capacity remains essentially constant with increasing flow-rate.

The trade-off between surface area and capacity as well as capacity versus flow-rate is a strong function of the size and diffusivity of the probe. A comparison of Figs. 4 and 5 show the dramatic effect of using a larger protein (BSA) to probe dynamic accessibility of binding sites. The Oligo R3 sample breakthrough capacity shows a steep drop-off with increased flow-rate, to the point of behaving like a pellicular support (i.e., binding only to the outer surface of the resin) at velocities beyond 3000 cm/h. The POROS R1 and POROS R2 capacities are roughly the same as with lysozyme (calculated as mg/ml), and although some modest decrease in breakthrough capacity is observed with flow-rate, they stabilize at about 85% and 75% of saturation capacity (POROS R1 and POROS R2, respectively).

This trend is even more pronounced for an even larger protein probe (hIgG), as shown in Fig. 6. The Oligo R3 breakthrough capacity drops more precipitously with flow-rate, such that at about 700 cm/h it is only 3 mg/ml. Once again, the breakthrough capacities, at the higher flow-rates, of POROS R1 and POROS R2, are seen to stabilize after a modest decrease. The combination of higher capacity for

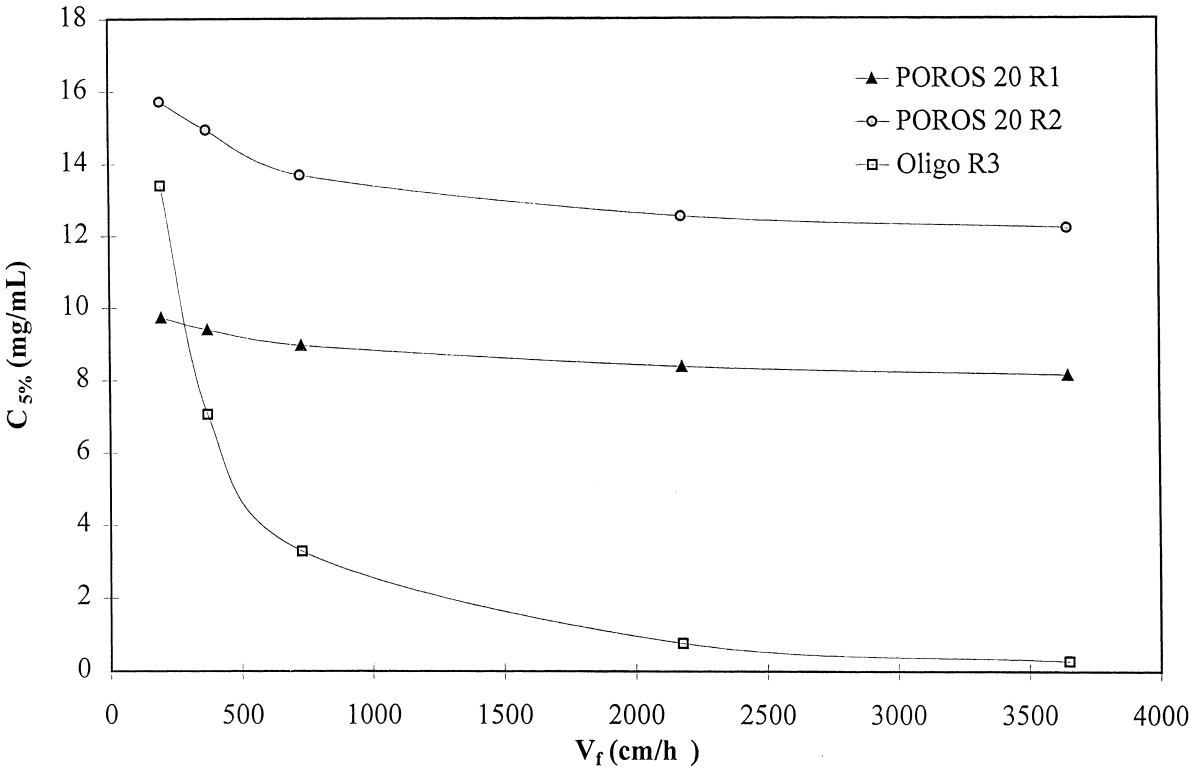

Fig. 6. Dynamic capacity comparisons using human γ-immunoglobulin (hIgG). The dynamic capacity of POROS R1 and POROS R2 and Oligo R3 is shown as a function of flow-rate. The properties of hIgG relative to lysozyme and BSA are shown in Table 1. The difference in the breakthrough capacity of the perfusive resins and the non-perfusive Oligo R3 is seen as the effect of convective enhancement in capture mode.

larger biomolecules and the ability to operate columns at elevated flow-rates, provides the basis for increased process throughput. The relative capacity difference between the higher surface area and lower surface area particles decreased with increasing protein size. This result suggests that a portion of the surface area of the Oligo R3 particles is not accessed by larger proteins. Fig. 7 shows the results of the frontal loading experiments for POROS R1 and Oligo R3, comparing lysozyme and hIgG as probes. The frontals are virtually superimposable for the POROS R1, at all flow-rates, for both probes. The frontal shape for Oligo R3, on the other hand, shows a marked dependence on flow-rate, especially with larger proteins.

The dynamic ratio (dr), defined as the 5% breakthrough capacity at high flow-rate (2000 cm/h) normalized to the 50% breakthrough at low flow-rate (200 cm/h), is used to further quantify the effect of perfusion in frontal mode.

$$\mathrm{dr} = \frac{C_{5\%}\ (2000\ \mathrm{cm/h})}{C_{50\%}\ (200\ \mathrm{cm/h})} \tag{13}$$

Table 3 lists the dynamic ratios for POROS R1, POROS R2 and Oligo R3, using lysozyme, BSA and IgG, and shows a clear correlation with calculated intraparticle permeabilities and split ratios. It is interesting to note that a relatively small split ratio (<0.001) provides sufficient convective flow to significantly enhance solute transfer rates, and hence, provide far superior capture efficiency.

The step-wise conversion of the crosslinked poly-

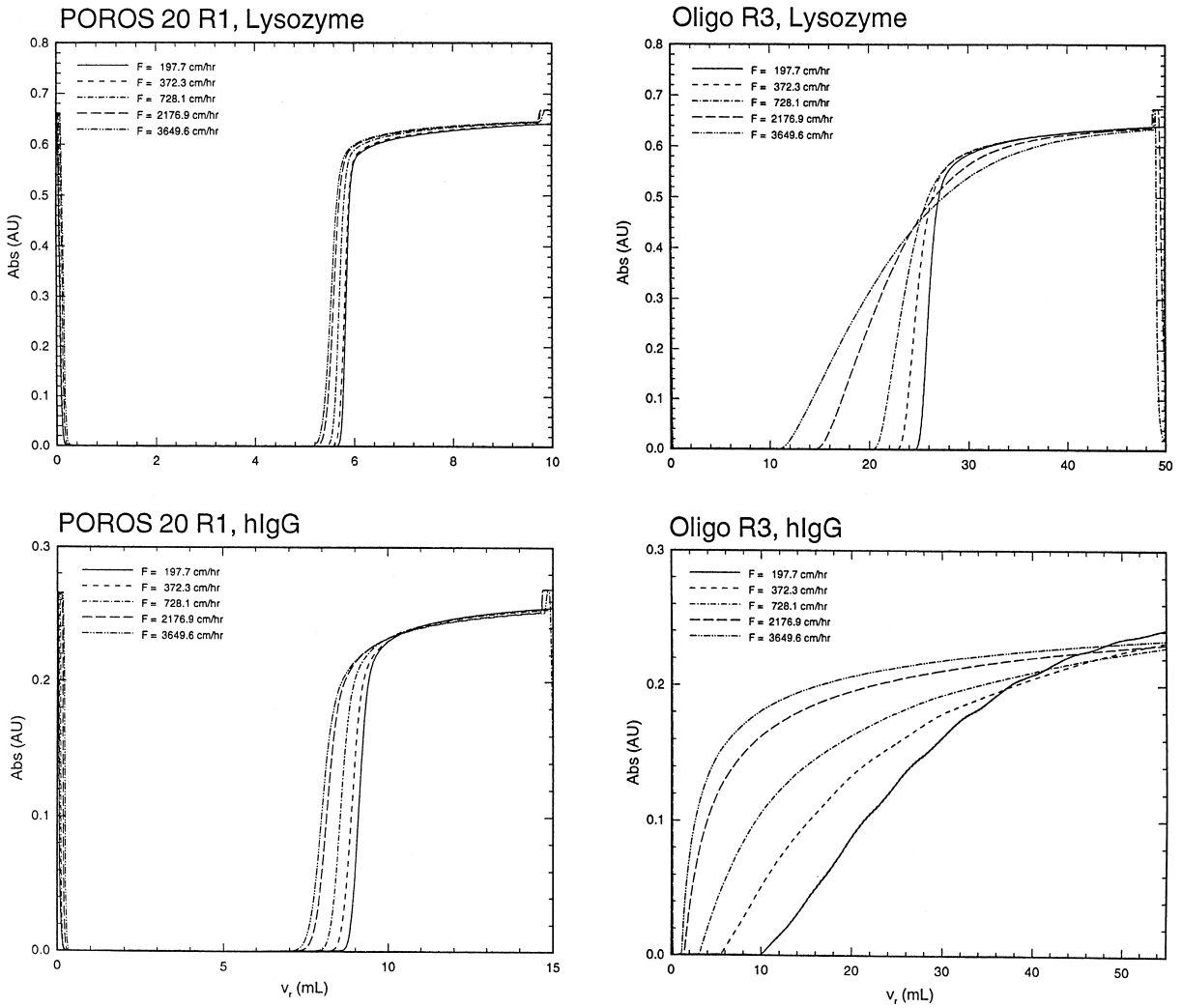

Fig. 7. Frontal curves for POROS R1 and Oligo R3. Each of the panels is labeled to show the frontal curves generated using POROS R1 and Oligo R3, with both lysozyme and hIgG. The perfusive POROS R1 shows virtually superimposable frontal curves across a broad range of flow-rates for both proteins. Note that although the breakthrough volume of hIgG on Oligo R3 (lower right-hand panel) at the lowest flow-rate (198 cm/h) is only about 10 ml, that the saturation volume is estimated to be about 2.5-times higher. This is indicative of the mass transport limitations of diffusive resins when binding large biomolecules.

Table 3
Intraparticle permeability calculations

	ε_p	d_m (μm)	K_p (m^2)	$\alpha \times 100$	dr (lys)	dr (BSA)	dr (IgG)
POROS R1	0.61	0.60	$3.58 \cdot 10^{-15}$	0.71	0.90	0.77	0.82
POROS R2	0.65	0.31	$1.44 \cdot 10^{-15}$	0.19	0.86	0.73	0.76
Oligo R3	0.64	0.04	$0.02 \cdot 10^{-15}$	0.00	0.59	0.07	0.02

Intraparticle permeability (K_p) was calculated according to the Carmen–Kozeny equation (Eq. (11)). Volumetric split ratio (α), was measured and reported by McCoy et al. [12] for the same samples, and dynamic ratio is defined in Section 3.3. The split ratio is defined in Section 2.3.3. The values for ε_p and d_m are calculated using Eqs. (7) and (12), and data taken from Table 2.

styrene, POROS R, resins for reversed-phase chromatography to ion-exchange functionality has been previously described [13]. By this process it is possible to easily tailor surface properties, including selectivity and capacity, independently of the pre-established pore size distribution. One of the challenges, specifically associated with the concept of increasing ligand density and binding capacity, is to carefully control the coating thickness so as not to destroy the convective mass transport properties by either blocking throughpores or adding excessive diffusional resistance. POROS S and SP are prepared from the POROS R1 support using direct surface functionalization chemistry and amplified surface functionalization, respectively. Whereas POROS R1 has a reversed-phase mode binding capacity of about 5 mg/ml for lysozyme (expressed as mg of protein per ml of column, or bed volume), in the cation-exchange mode POROS S has a lysozyme capacity of about 12 mg/ml, and POROS SP has a capacity of about 40 mg/ml. POROS HS is designed with the same basic surface chemistry as POROS SP, using the POROS R2 support. POROS HS has a binding capacity of about 95 mg/ml for lysozyme. In all cases, a roughly 10-fold capacity increase is observed for the cation-exchange coated resin relative to the underlying POROS R support (e.g., POROS R1 vs. POROS SP, or POROS R2 vs. POROS HS), and the dynamic capacity is largely retained with increasing flow-rate. These results are summarized in Fig. 8, where the breakthrough capacities at 397 and 3574 cm/h are compared for each resin. POROS HS shows a more pronounced decrease in capacity with respect to flow-rate, due to the lower split ratio of the underlying POROS R2 support.

The breakthrough capacity as a function of linear

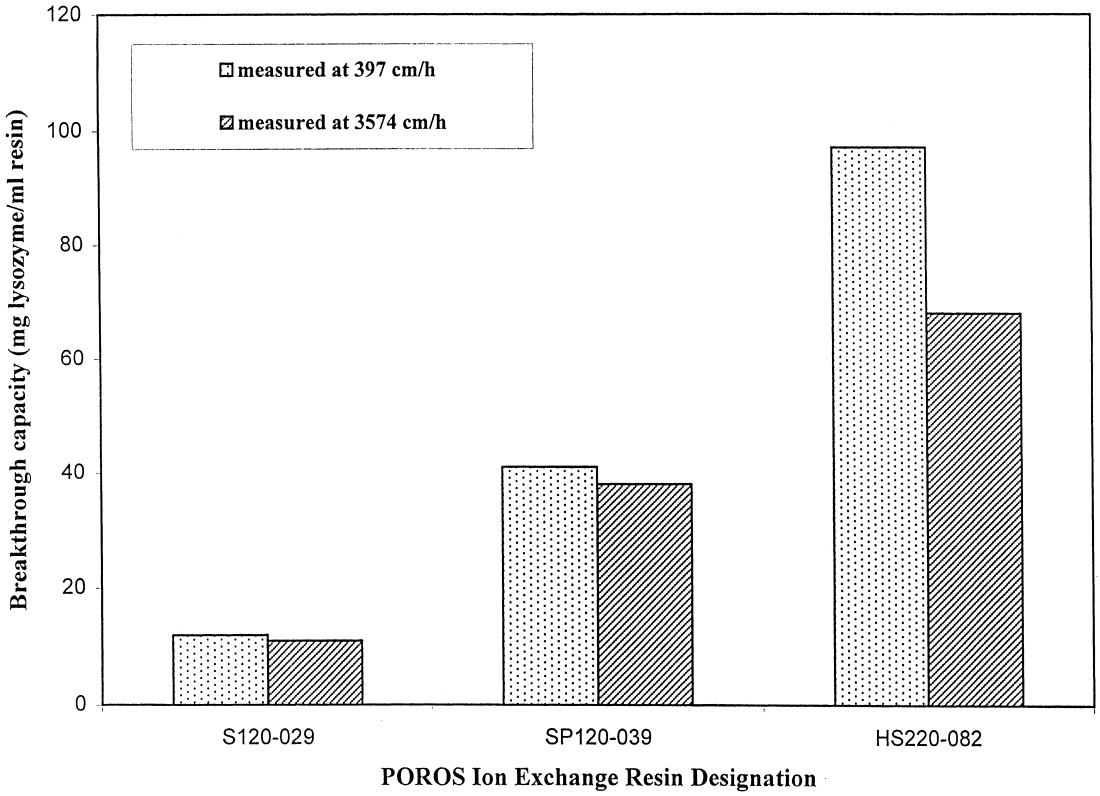

Fig. 8. Comparison of POROS ion exchanger dynamic capacities. Dynamic capacity was measured for three different POROS cation exchangers having different surface derivatizations. The POROS S and POROS SP are prepared on the POROS R1 support, whereas the POROS HS is prepared from the POROS R2.

velocity is plotted for POROS R1 and POROS SP in Fig. 9. The capacity is largely independent of flow-rate when measured for both lysozyme and IgG. In both cases, a 6–7-fold increase in binding capacity is observed for uncoated vs. coated phases, without incurring any significant penalty in dynamic accessibility of binding sites. A similar plot is shown for POROS HQ and POROS R1, using BSA, in Fig. 10. Here, the increase in anion-exchange binding capacity is about 10-fold. The high dynamic capacities of these POROS resins at elevated flow-rates has been verified by split ratio calculations [12] from zonal chromatography experiments. These values are reproduced in Table 4 for POROS R1, POROS R2, SP, and HQ, along with binding capacity values determined from the data plotted in Figs. 9 and 10. The split ratio values were estimated by fitting the column efficiencies, in a nonretained operating mode, as a function of flow-rate, to a perfusive van Deemter model [12]. Although a slight decrease in split ratio is estimated, for both SP and HQ chemistries, compared to POROS R1, the amount of convective enhancement is sufficient to offer dramatic improvements in capture efficiency over a purely diffusive support.

In the reversed-phase frontal experiments, Oligo R3 was used as the purely diffusive control. In the case of ion exchangers a commercially available 20 μm polymeric ion exchanger (HEMA-IEC BIO 1000 SB) was used as a purely diffusive model for comparison to POROS SP. This resin was chosen due to the similar particle size (20 μm) to the POROS samples in this study. Some of the physical properties of the HEMA resin, as measured by porosimetry and microscopy are shown in Table 5. Included in the Table are the calculated values for

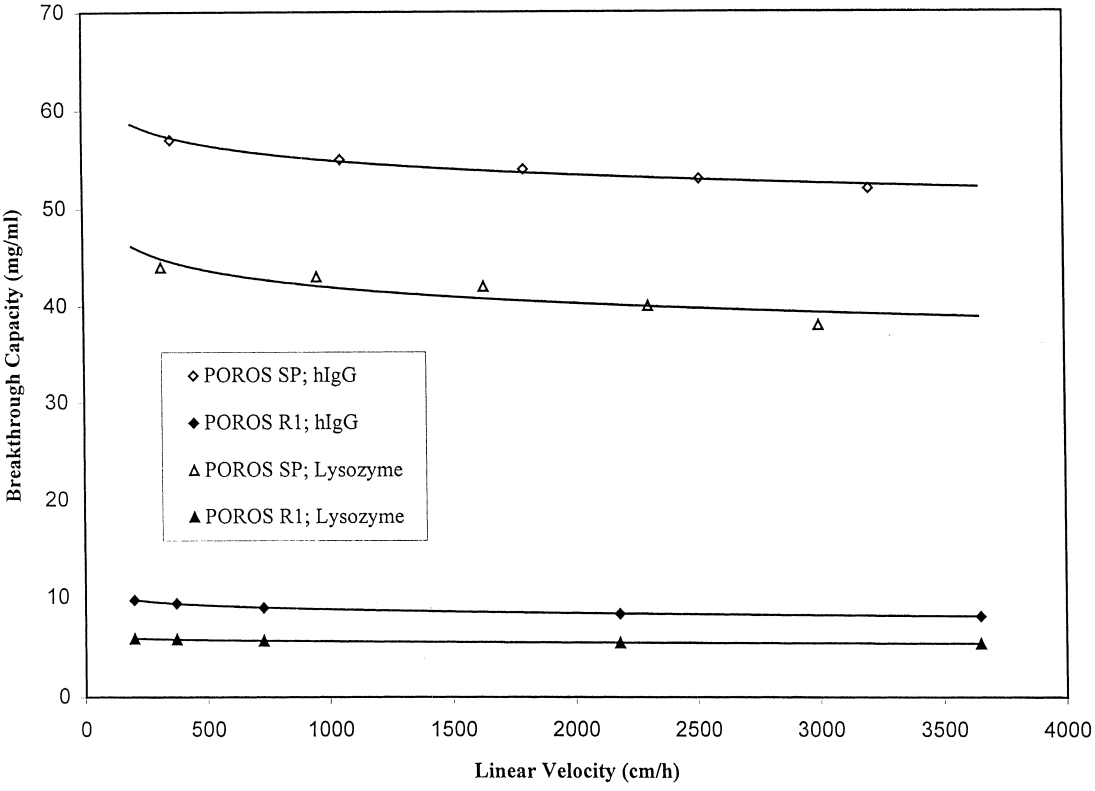

Fig. 9. Dynamic capacity plots of POROS R1 and POROS SP. A direct comparison of the dynamic capacity (measured at the 5% breakthrough point) as a function of flow-rate is made for POROS R1 and POROS SP using two proteins (lysozyme and hIgG). The comparison shows the increase in binding capacity imparted by the surface derivatization. Both the POROS R1 and the POROS SP show little dependence in dynamic capacity with flow-rate, due to the enhanced mass transport mechanism.

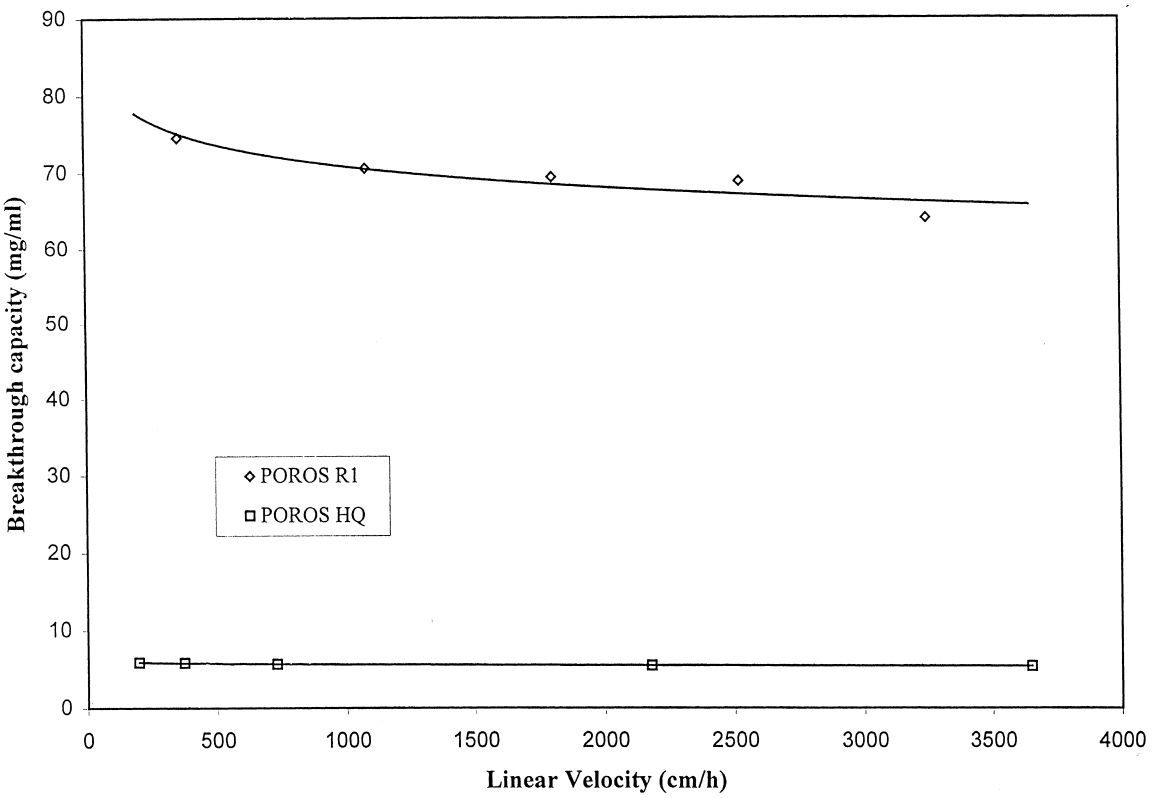

Fig. 10. Dynamic capacity plots of POROS R1 and POROS HQ. A direct comparison of the dynamic capacity (measured at the 5% breakthrough point) as a function of flow-rate is made for POROS R1 and POROS HQ using BSA. Both resins show only a small dependence of dynamic capacity on flow-rate. The POROS HQ anion exchanger has about 10× the binding capacity of the POROS R1 support from which it is derived.

intraparticle permeability (K_p) and split ratio (α) [12], confirming this material as purely diffusive with no possibility for intraparticle convective mass transfer. A comparison of the binding capacities of POROS SP and HEMA BIO 1000 SB, using hIgG, as a function of flow-rate is shown in Fig. 11. The capacity at both the breakthrough point of the frontal curve (5%) as well as the 50% point, are shown. Similar to the results for reversed-phase chromatography, protein binding capacity in the cation-exchange mode is insensitive to flow-rate for a perfusive particle, while the non-permeable particle demonstrates severe loss in capacity with increased flow-rate.

Table 4
Comparison of calculated split ratios and binding capacities

Media name	$\alpha \cdot 100$; protein probe	Capacity (mg/ml); protein
POROS R1	0.71; lysozyme	6.0; lysozyme
POROS R2	0.19; lysozyme	10.5; lysozyme
POROS SP	0.40; α-chymotrypsinogen	45; lysozyme
POROS HQ	0.50; α-chymotrypsinogen	52; BSA

By comparing POROS R1 and POROS R2 (reversed-phase supports), the effect of pore size on split ratio (α) and binding capacity is revealed. Comparison of the POROS R1 with POROS SP and HQ the effect of the added coating chemistry on the split ratio and binding capacity is seen. The capacities are measured in frontal mode as described in Section 2.3.3.

Table 5
The properties of diffusive ion-exchange resin (HEMA-IEC BIO 1000 SB)

$D_{particle}$	$25.9 \cdot 10^{-6}$ m
D_{pore}	$481 \cdot 10^{-10}$ m
ε_{pore}	0.296
A_{sp}	45.3 m^2/g
K_p	$0.003 \cdot 10^{-15}$ m^2
α	$6 \cdot 10^{-6}$

The characterization of the HEMA BIO 1000 SB as non-perfusive is supported by the values of the calculated split ratio (α) and particle permeability (K_p), below. $D_{particle}$ is measured by microscopy, and D_{pore}, A_{sp} and ε_{pore} taken from porosimetry data. The intraparticle permeability (K_p) is calculated as described in Section 3.2, using $d_m = 2d_{pore}$ (as in Table 3). The split ratio is calculated from a van Deemter model as previously described [12].

4. Conclusions

By variation of the pore size distribution in POROS perfusive particles, it is possible to control the intraparticle flow. Flow permeability of individual particles is unique to perfusive supports and can be simply related to characterization data (such as from pore size distribution measurements) according to the Carmen–Kozeny equation. The intraparticle permeability models are confirmed by comparison of measured physical properties to reported [15] values of direct intraparticle flow in POROS resins. Finally, the correlation of the degree of intraparticle flow on chromatographic performance is shown for the POROS R1 and POROS R2, relative to Oligo R3

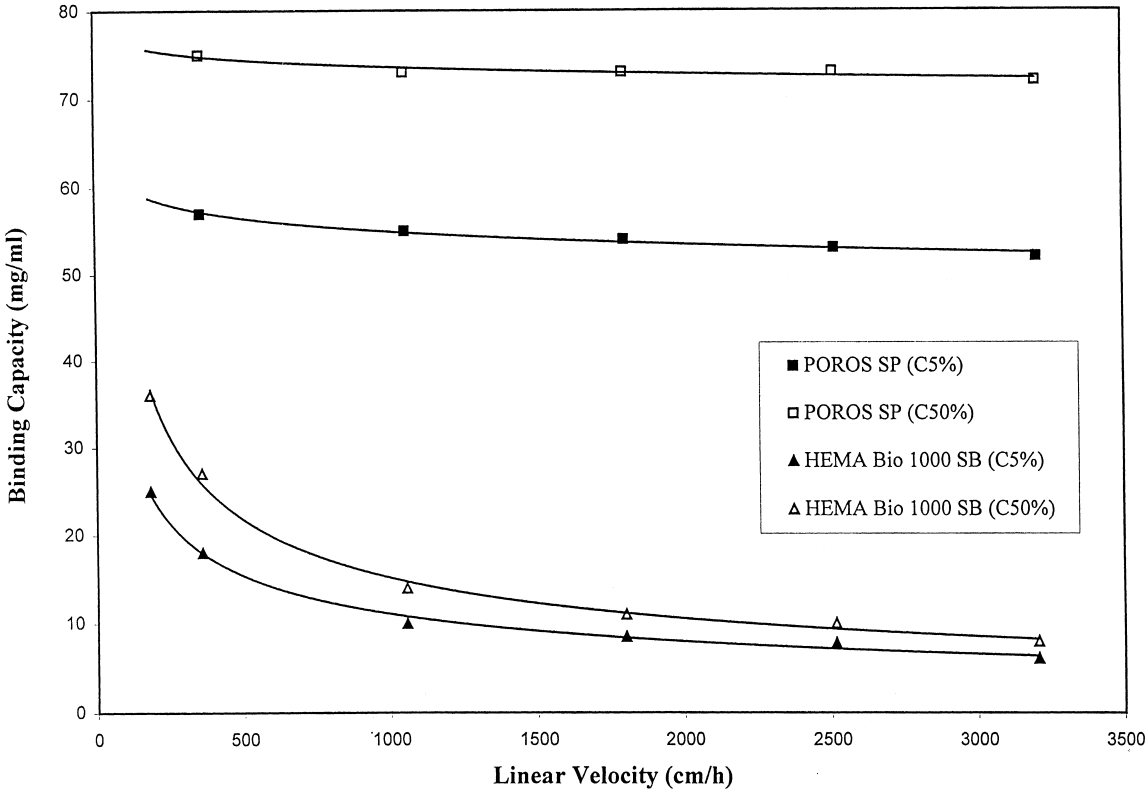

Fig. 11. Dynamic capacity comparison of POROS SP and a diffusive control resin. HEMA-IEC BIO 1000 SB, having a similar particle size and surface functionality as the POROS SP, was chosen as the diffusive control. The dynamic capacity is measured as described in Section 2.3.2. In this plot the dynamic capacity as measured at the 5% breakthrough point ($C_{5\%}$) and the 50% breakthrough point ($C_{50\%}$) is shown for each resin using lysozyme as the probe.

(used here as a non-perfusive control). Binding capacity, as an indicator of binding site accessibility, is shown to be largely independent of flow-rate for POROS R1 and POROS R2, using lysozyme, BSA and IgG as probes, whereas the Oligo R3 capacity drops off dramatically with increased flow. This is attributed to convective mass transport enhancement in the case of the POROS resins, and can be directly correlated to intraparticle flow, as defined in split ratio calculations, derived from zonal chromatography experiments. Correlation of pore size distribution and chromatographic mass transport properties is used to demonstrate how the latter can be controlled. However, the binding capacity of perfusive resins can be independently controlled by the application of coatings, assuming the coatings do not dramatically impair the mass transport properties.

It is possible to vary binding capacity of POROS ion exchangers, over a broad range, and independent of the pore structure and mass transport properties. Clear differences in dynamic capacity curves (i.e., breakthrough capacity plotted versus flow-rate) for both reversed-phase and ion-exchange resins are demonstrated for permeable and non-permeable particles. In all cases the capacities of POROS resins become independent of flow-rate in the perfusive regime, whereas non-permeable resins show a continual drop in binding efficiency with increased flow-rate. This experimental result confirms the predictions of mathematical models describing mass transport within the internal pore network of permeable and non-permeable particles.

It is also possible to estimate split flow ratios for perfusive supports, by fitting experimental data to mathematical models. The relative agreement of calculated particle permeability data, taken from physical property measurements, and split ratio values estimated by the models strengthens the mechanistic basis of the models and hence increases their predictive value. Using these models, split ratio values for coated resins (e.g., POROS SP and HQ) are shown to be in close agreement with the values derived for the underlying uncoated supports, indicating preservation of the beneficial mass transport properties of perfusive particles. In addition, the coated resins have a 5–10-fold higher binding capacity (depending on the derivatization chemistry) relative to the underlying supports from which they are made.

References

[1] J.J. van Deemter, F.J. Zuiderweg, A. Klinkenberg, Chem. Eng. Sci. 5 (1956) 271.
[2] N.B. Afeyan, N.F. Gordon, I. Mazsaroff, L. Varady, S.P. Fulton, Y.B. Yang, F.E. Regnier, J. Chromatogr. 519 (1990) 1.
[3] N. Afeyan, S. Fulton, N. Gordon, I. Maszaroff, L. Varady and F. Regnier, presented at the 9th International Symposium on HPLC of Peptides, Proteins and Polynucleotides, Philadelphia, PA, 6–8 Nov 1989.
[4] M.A. Stadalius, H.S. Gold, L.R. Snyder, J. Chromatogr. 327 (1985) 27.
[5] M.A. Stadalius, H.S. Gold, L.R. Snyder, J. Chromatogr. 327 (1985) 93.
[6] J.V. Dawkins, L.L. Lloyd, F.P. Warner, J. Chromatogr. 352 (1986) 157.
[7] R. Steffensen, J.J. Anderson, Biochromatogr. 2 (1987) 85.
[8] J. Frenz, W.S. Hancock, W.J. Henzel and Cs. Horváth, in K.M. Gooding and F.E. Regnier (Editors), HPLC of Biological Macromolecules, Methods and Applications (Chromatographic Science Series, Vol. 51), Marcel Dekker, New York, 1990, p. 145.
[9] K.D. Nugent, in C.T. Mant and R.S. Hodges (Editors), High-Performance Liquid Chromatography of Peptides and Proteins: Separation, Analysis and Conformation, CRC Press, Boca Raton, FL, 1991, p. 279.
[10] A.E. Rodrigues, A.M.D. Ramos, J.M. Loureiro, M. Diaz, Z.P. Lu, Chem. Eng. Sci. 47 (1992) 4405.
[11] G. Carta, M.E. Gregory, D.J. Kirwan, H.A. Massaldi, Sep. Technol. 2 (1992) 62.
[12] M.A. McCoy, K. Kalghatgi, F.E. Regnier, N.B. Afeyan, J. Chromatogr. 743 (1996) 221.
[13] L. Varady, N. Mu, Y.-B. Yang, J. Chromatogr. 631 (1993) 107.
[14] PoreSizer 9320: Operator's Manual version 2.00, Micromeritics, Norcross, GA, 22 March 1991.
[15] J. Pfeiffer, J. Chen, J. Hsu, AIChE J. 42 (1996) 932.
[16] K.A. Kun, R. Kunin, J. Polym. Sci., A-1 6 (1968) 2689.
[17] W.L. Sederel, G.J. de Jong, J. Appl. Polym. Sci. 17 (1973) 2835.
[18] H. Jacobelli, M. Bartholin, A. Guyot, Angew. Makromol. Chem. 80 (1979) 31.
[19] H. Jacobelli, M. Bartholin, A. Guyot, J. Appl. Polym. Sci. 23 (1979) 927.
[20] D.Y.D. Chung, M. Bartholin, A. Guyot, Angew. Makromol. Chem. 103 (1982) 109.
[21] O. Okay, E. Soner, A. Gungor, T.I. Balkas, J. Appl. Polym. Sci. 30 (1985) 2065.
[22] W. Rolls, F. Svec, J.M.J. Frechet, Polymer 31 (1990) 165.

[23] K. Haupke, V. Pientka, J. Chromatogr. 102 (1974) 117.
[24] A.I. Liapis, M.A. McCoy, J. Chromatogr. 599 (1992) 87.
[25] M.A. McCoy, A.I. Liapis, K.K. Unger, J. Chromatogr. 644 (1993) 1.
[26] A.I. Liapis, M.A. McCoy, J. Chromatogr. A 660 (1994) 85.
[27] A.E. Rodrigues, L. Zuping, J.M. Loureiro, Chem. Eng. Sci. 46 (1991) 2765.
[28] A.E. Rodrigues, J.C. Lopes, Z.P. Lu, J.M. Loureiro, M.M. Dias, J. Chromatogr. 590 (1992) 93.
[29] S. Fulton et al., BioTechniques 11 (1991) 226.
[30] A.J. Hunt, P. Lynch, T. Londo, P. Diamond, N.F. Gordon, T. McCormack, A. Schitz, M. Percoskie, X. Cao, J.P. McGrath, S. Putney, R.A. Hamilton, J. Chromatogr. A 708 (1995) 61.
[31] M.S. Roolbolza, S. Shochat, S.E. Tjus, A. Hagman, P. Gast, B. Anderson, Photosynthesis Res. 46 (1995) 339.
[32] H. Wajcman, R. Ducrocq, J. Riou, M. Mathis, C. Godart, C. Prehu, F. Galacteros, Anal. Biochem. 237 (1996) 80.
[33] N. Tanaka, Kyoto Institute of Technology, unpublished results.
[34] I. Halasz, K. Martin, Angew. Chem., Int. Ed. Engl. 17 (1978) 901.
[35] W. Werner, I. Halasz, J. Chromatogr. Sci. 18 (1980) 277.
[36] J.H. Knox, H.P. Scott, J. Chromatogr. 316 (1984) 311.
[37] J.H. Knox, H.J. Ritchie, J. Chromatogr. 387 (1987) 65.
[38] A.E. Rodrigues, C. Chenou, M. Rendueles de la Vega, Chem. Eng. J. 61 (1996) 191.
[39] W. Kopaciewicz, S.P. Fulton, S.Y. Lee, J. Chromatogr. 409 (1988) 111.
[40] A.E. Rodrigues, B.J. Ahn, A. Zoulalian, AIChE J. 28 (1982) 541.
[41] H.A. Sorber (Editor), Handbook of Biochemistry, Selected Data for Molecular Biology, CRC Press, Cleveland, OH, 1970.